Hindawi Publishing Corporation
Journal of Applied Mathematics
Volume 2012, Article ID 245702, 21 pages
doi:10.1155/2012/245702

Research Article

Numerical Simulation of Sloshing Phenomena in Cubic Tank with Multiple Baffles

Mi-An Xue,[1,2] Jinhai Zheng,[1,2] and Pengzhi Lin[3]

[1] *State Key Laboratory of Hydrology-Water Resources and Hydraulic Engineering, Hohai University, Nanjing 210098, China*
[2] *College of Harbour, Coastal and Offshore Engineering, Hohai University, Nanjing 210098, China*
[3] *State Key Laboratory of Hydraulics and Mountain River Engineering, Sichuan University, Chengdu 610065, China*

Correspondence should be addressed to Jinhai Zheng, jhzheng@hhu.edu.cn
and Pengzhi Lin, cvelinpz@scu.edu.cn

Received 20 January 2012; Revised 17 April 2012; Accepted 30 April 2012

Academic Editor: Carl M. Larsen

A two-phase fluid flow model solving Navier-Stokes equations was employed in this paper to investigate liquid sloshing phenomena in cubic tank with horizontal baffle, perforated vertical baffle, and their combinatorial configurations under the harmonic motion excitation. Laboratory experiment of liquid sloshing in cubic tank with perforated vertical baffle was carried out to validate the present numerical model. Fairly good agreements were obtained from the comparisons between the present numerical results and the present experimental data, available numerical data. Liquid sloshing in cubic tank with multiple baffles was investigated numerically in detail under different external excitation frequencies. Power spectrum of the time series of free surface elevation was presented with the aid of fast Fourier transform technique. The dynamic impact pressures acting on the normal and parallel sidewalls were discussed in detail.

1. Introduction

The effect of severe sloshing motion on global seagoing vessels is an important factor in safety design of such containers. The violent motion of fuel or liquid cargo in tanks may result in severe sloshing loads on the containment system and supporting structure. It is important to quantify the effects of this sloshing on the system for design consideration. Even simple baffles reduce sloshing effects by dissipating kinetic energy due to the production of vortices into the fluid; their exact shapes and positions need to be designed with the use of numerical model simulation or physical testing. Nonetheless, the damping mechanisms of baffle are still not fully understood. Moreover, liquid sloshing in containers is an important phenomenon

of great practical application with regard to the safety of space vehicles, storage tanks, road vehicle tanks, ships, and elevated water towers under ground motion and remains of great concern to aerospace, civil, nuclear engineers, physicists, designers of road tankers and ship tankers, and mathematicians [1]. The studies of liquid sloshing in a tank with baffles are still very necessary.

Liquid sloshing phenomenon has been investigated extensively using various numerical model [2] and experimental setup in the past few decades. Faltinsen [3] developed a boundary element method (BEM) model to study liquid sloshing problems. Koh et al. [4] developed a coupled BEM-FEM for the dynamic analysis of rectangular liquid storage tanks including free surface sloshing motion. Chen and Chiang [5] analyzed the interaction effect between the fully nonlinear sloshing fluid and the floating tank associated with coupled surge, heave and pitch motions. Dodge [6] offered more valuable results on lateral sloshing in moving containers in spacecraft applications. Forbes [7] studied the motion of an ideal fluid in a rectangular tank under horizontal sinusoidal periodic forcing excitation.

Fluid motion in partially filled tanks is prone to have a big impact on the forces acting on the tank walls when the frequency of tank-forced motion is close to a natural frequency of fluids inside the tank or the external excitation amplitude is very large. The damping of sloshing is therefore a key issue in liquid-filled tanker design. Keulegan and Parkinson [8] studied the inertia and drag coefficient of cylinders and plates in an oscillating fluid. Miles [9] analyzed the damping effects of ring baffle and obtained an analytical solution for damping ratio in terms of tank dimensions and sloshing height amplitude for circular-cylindrical tanks when the liquid height is considerably greater than the tank radius. Armenio and La Rocca [10] analyzed sloshing of water in rectangular open tanks and observed that the presence of a vertical baffle at the middle of the tank dramatically changed the sloshing response. Kim [11] simulated liquid sloshing in 2D and 3D liquid containers with and without baffle using finite difference method (FDM). Akyildiz and Çelebi [12] investigated pressure distribution in a rigid rectangular tank due to large amplitude liquid sloshing. In their studies, different cases including baffled and unbaffled tanks with different filling levels were computed in the vicinity of the natural frequency. Çelebi and Akyildiz [13] studied a nonlinear sloshing inside a partially filled rectangular tank with and without baffle. Akyildiz and Ünal [14] conducted an experimental study on pressure variations and 3D effects due to liquid sloshing in a baffled tank under pitch excitation. Cho et al. [15] investigated the effects of baffle on liquid sloshing in a 2D baffled tank subjected to forced excitation by using finite element method (FEM). Biswal et al. [16] studied the influence of annular baffle on nonlinear sloshing in both cylindrical and rectangular tank using FEM. The results indicate that the baffle has greater influence on the slosh frequencies of liquid when placed near to the liquid free surface, and the influence is gradually reduced when it is moved towards the bottom of the tank.

Baffle with orifice can be found in some contemporary road tankers carrying fuel oils or liquefied natural gas (LNG). This kind of baffle can allow the lower surface liquid to pass through, thus attenuating the impact forces on the baffle. Younes et al. [17] conducted an experimental study of the hydrodynamic damping provided by using vertical baffles with orifice in partially filled rectangular tanks; they pointed out that the size, location, number, and drilling holes of the vertical baffle significantly influence the hydrodynamic damping. Panigrahy et al. [18] developed a slosh experimental setup with a degree of freedom (DOF) of horizontal motion to estimate pressure distribution on tank walls and surface elevation variation in a tank with drilled orifice baffle. Eswaran et al. [19] numerically investigated the effects of baffles with different shapes and arrangements on a partially filled cubic tank using the automatic dynamic incremental nonlinear analysis (ADINA) software.

In the present study, liquid sloshing in cubic tank with horizontal baffle, perforated vertical baffle and their combination are investigated numerically to explore the effects of baffle with different shapes and arrangements on reducing liquid sloshing. A virtual boundary force (VBF) method [20] by using the idea of applying momentum forces, which stems from the immersed boundary (IB) method [21] but can handle the surface-piercing structures, is adopted and combined with the volume-of-fluid (VOF) method in this study to investigate liquid sloshing in three-dimensional (3D) rectangular tank with internal baffles. A two-phase fluid flow model is employed to solve the spatially averaged Navier-Stokes equations in a noninertial reference frame. The resulting pressure Poisson equation revised by VBF method is solved by the two-step projection method with the aid of Bi-CGSTAB technique, and the large-eddy simulation (LES) technique is used for turbulence modeling.

2. Mathematical Model and Numerical Approach

In this study, an in-house code [22] is employed for all numerical predictions. The three-dimensional incompressible liquid sloshing motions in a tank are governed by the spatially averaged Navier-Stokes (SANS) equations, continuity equation and transportation equation of density. The Smagorinsky subgrid-scale (SGS) turbulence model is applied, so the SANS equations can be written in tensor form as follows:

$$\frac{\partial \overline{u}_i}{\partial x_i} = 0, \tag{2.1}$$

$$\frac{\partial \overline{u}_i}{\partial t} + \frac{\partial \overline{u}_i \overline{u}_j}{\partial x_j} = -\frac{1}{\rho}\frac{\partial \overline{p}}{\partial x_i} + \frac{\partial}{\partial x_j}\left[(\nu + \nu_t)\left(\frac{\partial \overline{u}_i}{\partial x_j} + \frac{\partial \overline{u}_j}{\partial x_i}\right)\right] + f_i, \tag{2.2}$$

$$\frac{\partial \rho}{\partial t} + \overline{u}_i \frac{\partial \rho}{\partial x_i} = 0, \tag{2.3}$$

where $i, j = 1, 2, 3$ for three-dimensional flows, $\overline{u}_i$ denotes the ith filtered velocity component, ρ is the liquid density, ν is the kinematic viscosity, $\overline{p}$ is the filtered pressure, and the f_i is the external body force. Once the rate of the strain tensor $\overline{\sigma}_{ij} = (\partial \overline{u}_i/\partial x_j + \partial \overline{u}_j/\partial x_i)/2$ is defined in this model, the molecular viscous stress tensor $\overline{\tau}_{ij} = 2\rho\nu\overline{\sigma}_{ij}$ is obtained here. The symbol "−" denotes spatially averaged and can be dropped herein for simplicity. Especially the stress $R_{ij} = 2\rho\nu_t\overline{\sigma}_{ij}$ is modeled by the SGS turbulence model from the concept of LES, where $\nu_t = l_s^2\sqrt{2\overline{\sigma}_{ij}\overline{\sigma}_{ij}}$ is the eddy viscosity and l_s is the characteristic length scale which is proportional to the filter width $\sqrt[3]{\Delta x \Delta y \Delta z}$ through the Smagorinsky coefficient $c_s = 0.15$ [23]. In LES, the larger 3D unsteady turbulent motions are directly represented, whereas the effects of the smaller-scale motions are modeled. LES can be therefore expected to be more accurate and reliable than Reynolds-stress models for flows in which large-scale unsteadiness is significant.

The vector form of external body force f_i is as follows [24]:

$$\vec{f} = \vec{g} - \frac{d\vec{U}}{dt} - \frac{d\dot{\vec{\theta}}}{dt} \times \left(\vec{r} - \vec{R}\right) - 2\dot{\vec{\theta}} \times \frac{d\left(\vec{r} - \vec{R}\right)}{dt} - \dot{\vec{\theta}} \times \left[\dot{\vec{\theta}} \times \left(\vec{r} - \vec{R}\right)\right], \tag{2.4}$$

where $\vec{g}$, $\vec{U}$, and $\dot{\vec{\theta}}$ are the gravitational acceleration, translational and rotational velocity of the noninertial coordinate, respectively; $\vec{r}$ and $\vec{R}$ are the position vector of the considered point and rotational motion origin O. The second term of the right-hand side is the translational inertia, while the third, fourth, and fifth terms are due to the rotational motion, which are referred to as the angular acceleration, Coriolis force, and Centrifugal force, respectively.

In order to model the internal baffle, the VBF method is adopted here. In the VBF method, an additional virtual boundary force $(F_{\mathrm{VBF}})_i$, which is to replace the actual reaction force and is only nonzero on the solid surface, is applied in the SANS equations. The definition of the $(F_{\mathrm{VBF}})_i$ is as follows:

$$(F_{\mathrm{VBF}})_i = \begin{cases} \dfrac{u_i^{n+1} - \tilde{u}_i^{n+1}}{\Delta t} + \dfrac{1}{\rho^n}\dfrac{\partial p^{n+1}}{\partial x_i} - f_i & \text{virtual boundary} \\ 0 & \text{elsewhere.} \end{cases} \tag{2.5}$$

The detailed numerical implementations to determine the $(F_{\mathrm{VBF}})_i$ can be found in our previous works [20, 25].

The VOF interface tracking method is used to track the free surface. By introducing a VOF function F,

$$F = \frac{\rho - \rho_g}{\rho_l - \rho_g}, \tag{2.6}$$

where ρ_g is density of gas and ρ_l is density of liquid. Equation (2.3) becomes

$$\frac{\partial F}{\partial t} + \overline{u}_i \frac{\partial F}{\partial x_i} = 0, \tag{2.7}$$

where F represents the volumetric fraction between the gas and liquid, which equals to 0 in gas and 1 in liquid. In the VOF method, the second-order piecewise linear interface calculation is used to reconstruct the interface and to determine the VOF fluxes; the normal vector of the interface in each grid is calculated using Youngs' least squares method [26]. The details of the numerical procedures can be found in Liu [27].

In the study, an FDM is applied to solve the governing equations. Tank volume is discretized into the Cartesian staggered grid system, as shown in Figure 1. The velocity components are defined at the centers of cell boundaries; pressure and VOF function is calculated at the center of the cell. The forward time difference method is used to discretize the time derivative, and the central difference method is employed to discretize the pressure gradient terms. The convection terms are discretized by the combination of the central difference method and upwind method; taking the term $(\partial u/\partial x)_{i+1/2,j,k}$, for example,

$$\left(\frac{\partial u}{\partial x}\right)_{i+1/2,j,k} = \frac{\left\{\left[1 + \alpha\,\mathrm{sgn}\left(u_{i+1/2,j,k}\right)\right]\Delta x_{i+1}(\partial u/\partial x)_{i,j,k} + \left[1 - \alpha\,\mathrm{sgn}\left(u_{i+1/2,j,k}\right)\right]\Delta x_i(\partial u/\partial x)_{i+1,j,k}\right\}}{\Delta x_\alpha}, \tag{2.8}$$

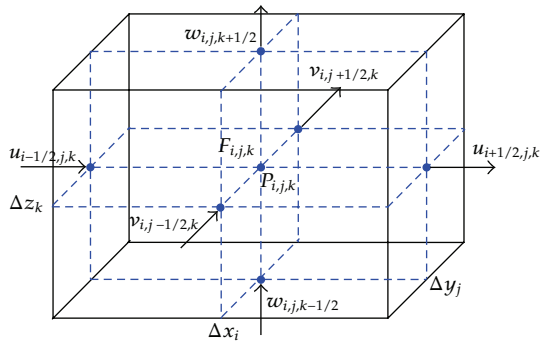

Figure 1: The definition of physical quantity in the Cartesian staggered grid.

where $\Delta x_\alpha = \Delta x_{i+1} + \Delta x_i + \alpha \operatorname{sgn}(u_{i+1/2,j,k})(\Delta x_{i+1} - \Delta x_i)$, the coefficient α is weight factor between the upwind scheme and the central difference scheme. The finite difference form becomes the central difference when $\alpha = 0$; the finite difference form becomes the upwind scheme when $\alpha = 1$. In this study, the value of the coefficient $\alpha = 0.3$ is used in the following simulations. Two-step projection method is employed here to solve the SANS equations; the details of numerical procedure are similar to that described in Xue and Lin [25]. In the initial numerical simulation, all the liquid was assumed to be at rest. The boundary conditions of no-slip velocity and zero normal pressure gradients are applied on the liquid-solid interfaces.

3. Model Validations

3.1. 2D Sloshing in Tank with Horizontal Baffle under Surge Excitation

Baffles are widely used as slosh suppression devices in the liquid storage containers. However, baffle damping effectiveness depends upon dimension and orientation of the baffle installed into a tank. Biswal et al. [16] investigated the effects of a horizontal baffle on the slosh response by varying its position and length via solving Laplace equation using a mixed Eulerian-Langrangian FEM. In their study, three different horizontal baffles in length will be selected here to compare with the present numerical results. The length of the rectangular tank is 1.0 m, and the liquid depth in the tank is 0.5 m. The tank is subjected to sinusoidal horizontal acceleration: $\ddot{x} = -a\omega^2 \sin \omega t$, where excitation amplitude $a = 0.002$ m and excitation frequency $\omega = 5.29$ rad/s. The ratio W/L of horizontal baffle length versus tank length is taken as 0.4, 0.6, and 0.8, respectively. The baffle is located at a depth of $b = 0.8h$ from the initial free surface and on the left boundary of the tank, as shown in Figure 2. The baffle is 0.005 m in thickness, which is made of PVC and is assumed to be rigid. The employed grid system in our simulation has 50 uniform horizontal meshes with $\Delta x = 0.02$ m and 63 nonuniform vertical meshes with 20 grids of the minimum mesh size $\Delta z = 0.006$ m being deployed in the vicinity of the free liquid surface.

Comparisons of the time history of free surface sloshing response at the right wall of the tank between the present numerical results and the numerical data of Biswal et al. are plotted in Figure 3 for various W/L ratios. Good agreements are obtained. It is observed from Figure 3 that the nonlinear liquid sloshing amplitude at the right tank wall decreases with

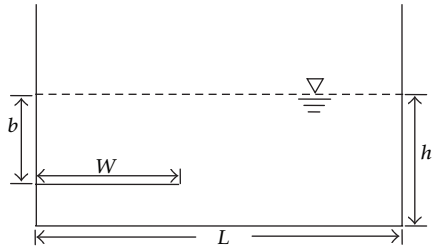

Figure 2: Rectangular tank with a horizontal baffle.

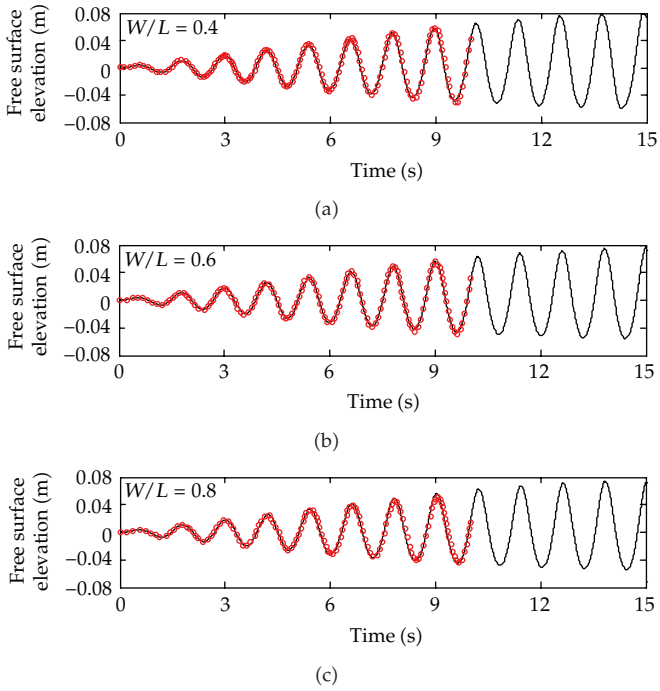

Figure 3: Comparisons of the time history of free surface elevation at the right wall of the baffled tank between the present numerical results (solid line) and the numerical data of Biswal et al. [16] (circle).

the increase in the W/L ratio. One of possible damping mechanisms is that the increasing baffle surface area suppresses the vertical velocity of more slosh fluids, as shown in Figure 4.

3.2. 3D Sloshing in Tank with Perforated Vertical Baffle under Surge Excitation

In this section, an experiment of liquid sloshing in cubic tank with perforated vertical baffle under different excitation frequencies was carried out in State Key Laboratory of Hydraulics and Mountain River Engineering at Sichuan University in China. The cubic Perspex tank of interior length 570 mm, width 310 mm, and height 700 mm was fixed on a shaking table that could move horizontally on linear bearings. Oscillatory movement of the shaking table was driven by an irregular wave-maker system [25], which can produce all kinds of harmonic and

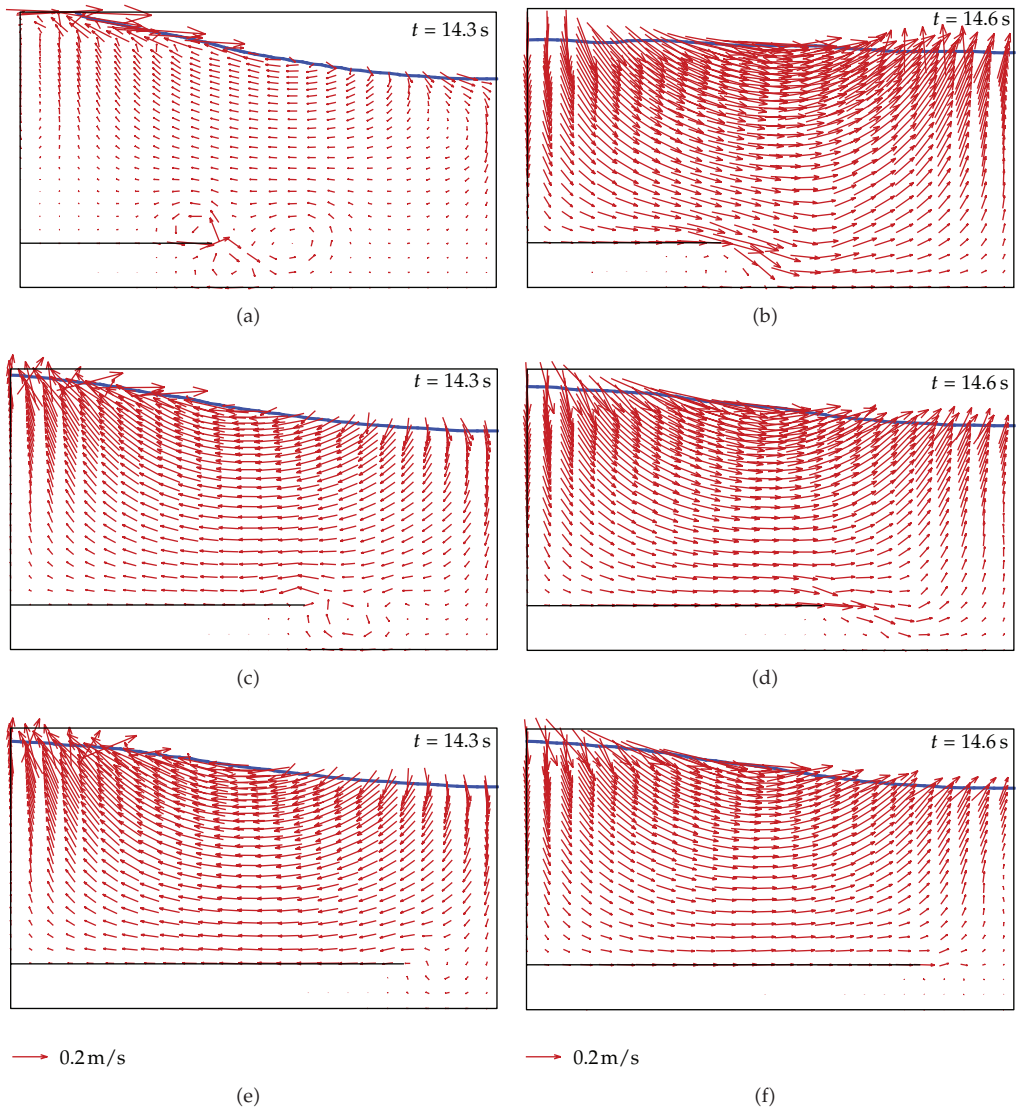

Figure 4: Velocity fields of liquid sloshing in a tank with different horizontal baffle in length.

random motion such as cosine function and JONSWAP spectra. In this study, only the pure cosine motion of the wave-maker was used; the available random motion would be used for future experimental investigations on nonlinear liquid sloshing using this apparatus.

The experimental apparatus and baffle configuration is shown in Figure 5. Three wave gauge sensors are employed to record the free surface elevation with time. Two pressure transducers are used to obtain the slosh-induced impact pressure acting on the right tank wall. The vertical baffle with square orifice with 250 mm in height, 310 mm in width, and 6 mm in thickness is mounted on the center of bottom of the tank. The square orifice of length 80 mm is made of rigid Perspex, whose center locates at 35 mm on the central upper part of the vertical baffle. The working fluid that was used in the experiment reported here was water

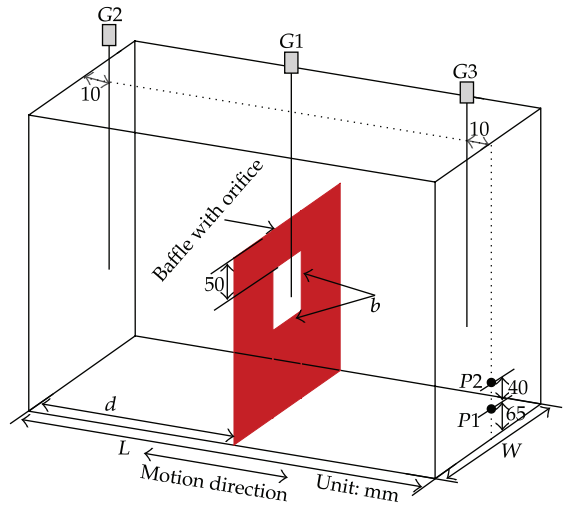

Figure 5: Schematic diagram of wave gauges, pressure transducers and slosh suppression baffle arrangement.

at room temperature. The water depth was 280 mm, so the lowest natural frequency is $\omega_0 = 7.0247\,\text{rad/s}$ according to the dispersion equation $\omega_n^2 = kg\tanh kh$, where $k = (2n+1)\pi/L$, L is tank length, h is water depth, and n is the mode number. The tank motion is the surge oscillations along the x-axis, which follows the cosine function given as $x = -a\cos\omega t$, where $a = 15\,\text{mm}$ and $\omega = 0.5\omega_0$ are the external excitation amplitude and frequency, respectively.

Experiment and numerical simulation of liquid sloshing in cubic tank with perforated vertical baffle are synchronously considered here. In the simulation, the 3D grid system has 114×62 uniform horizontal meshes with the mesh size $\Delta x = \Delta y = 5\,\text{mm}$ and 70 nonuniform vertical meshes with 20 grids being arranged near the free surface in which the minimum mesh size is $\Delta z = 2\,\text{mm}$. Figure 6 shows the comparisons of the free surface elevation at three wave gauges and the pressure at two pressure transducers between the experimental data and the numerical simulation results. Fairly good agreements are obtained at all measurement points, indicating that the present model is an accurate tool in investigating the liquid sloshing phenomenon in a tank with baffles.

4. Numerical Simulation of Liquid Sloshing in Cubic Tank with Multiple Baffles

4.1. Problem Description

Slosh suppression in moving liquid storage containers is considered to be one of the major key issues in engineering designs. One approach to slosh suppression of such systems partially filled by liquids is through energy dissipation using a partition or baffle. The conventional horizontal baffles or vertical baffles are already in use for slosh suppression of liquefied natural gas (LNG) containments. The nonconventional vertical baffle perforation may offer substantial advantages in terms of both increased damping effectiveness and reduced baffle weight. However, the damping provided by the perfected baffle depends upon the orifice size, number, location and excitation frequency, and so forth.

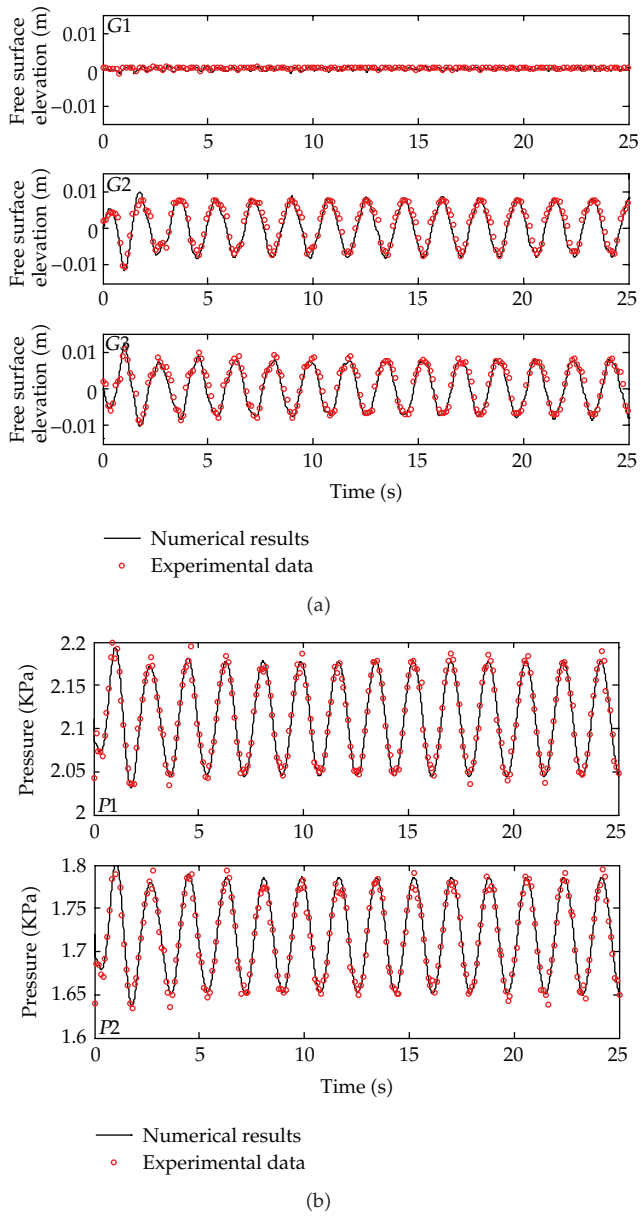

Figure 6: Comparisons of (a) free surface elevation at three wave gauges and (b) pressure at two pressure transducers between the experimental data and the numerical results for sloshing in a tank with perforated vertical baffle ($x = -a\cos\omega t$, $a = 15$ mm, $\omega = 0.5\omega_0$).

In the present study, for investigating the damping effectiveness of perforated vertical baffle, four same square orifices of length b are drilled on each vertical baffle. The combinatorial arrangements of two horizontal baffles and two perforated vertical baffles in a symmetric cubic tank are shown in Figure 7. Two horizontal baffles with 120 mm in width are mounted on the tank wall side and at the same height of $H_b = 220$ mm but opposite position. Two vertical baffles with 200 mm in width are installed on the bottom and at the center of the tank.

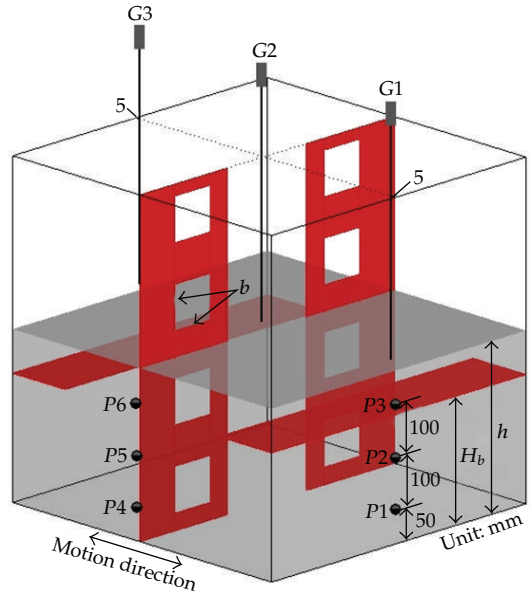

Figure 7: Schematic of liquid sloshing in cubic tank with horizontal baffles and orifice vertical baffles.

The square orifice length b is selected to be equal to 0 mm, 40 mm, and 80 mm, respectively. Three numerical wave gauges, which are located at the center, 5 mm near the left and right boundary of the tank, are used to record the free surface elevation with time. Six numerical pressure gauges are used to obtain the slosh-induced impact pressure acting on the sidewalls normal and parallel to the motion direction of the tank. For cubic tank, the (n, m) wave modes have the corresponding natural frequency that is determined by the dispersion equation:

$$\omega_{mn}^2 = \sqrt{\left(\frac{mg\pi}{L_x}\right)^2 + \left(\frac{ng\pi}{L_y}\right)^2} \tanh \sqrt{\left(\frac{m\pi h}{L_x}\right)^2 + \left(\frac{n\pi h}{L_y}\right)^2} \quad (m, n = 0, 1, 2, \ldots). \tag{4.1}$$

The tank dimension is $L_x = L_y = 600$ mm, and the water depth is $h = 300$ mm, so that 50% of the tank is filled with water. The length and width of the tank was chosen to be equal to obtain the symmetric behavior of the cubic tank in this study. So, the lowest natural frequency is $\omega_{10} = \omega_{01} = 6.8636$ rad/s due to the symmetry of the cubic tank. The computational domain is discretized by 120×60 uniform meshes with the mesh size $\Delta x = 5$ mm and $\Delta y = 10$ mm in the horizontal plane and 100 nonuniform vertical meshes with 20 meshes being arranged near the free surface, where the minimum mesh size is $\Delta z = 3$ mm. The horizontal excitation velocity of the tank follows cosine function, that is, $u = -A \cos \omega t$ for $t \geq 0$, where $A = a\omega$ is the velocity amplitude with $a = 5$ mm being the displacement amplitude and ω is the angular frequency of the excitation. In the following simulations, the excitation frequency ω would be chosen as π and 6.8636 rad/s, respectively.

4.2. Free Surface Elevation and Power Spectrum

In this section, several numerical experiments are performed in the same cubic tank for investigating the effect of combinatorial baffles on reducing liquid sloshing. In the simulation of $\omega = \pi$ rad/s being away from the lowest natural frequency of liquid-tank system, the numerical results of free surface elevation η at three wave gauges are plotted in Figure 8 for liquid sloshing in cubic tank with different baffle arrangements. It is shown that the effectiveness of different combinatorial baffles on reducing liquid sloshing amplitude is no apparent difference and slight when the external excitation frequency is away from the resonant frequency. However, the natural frequency has been shifted due to the presence of the baffles. The quantitative data are clearer in the power spectrum of the time series of the free surface elevation at wave gauge $G1$. The input data of 30 s with sampling interval 0.01 s were used to obtain the power spectrum with the aid of the fast Fourier transform (FFT) technique.

Figure 9 shows the power spectrum for liquid sloshing in a tank without baffle, with vertical baffles and horizontal baffles, with small orifice baffles and horizontal baffles, and with big orifice baffles and horizontal baffles, respectively. The first peak frequency of the power spectrum is 0.4998 Hz for four different baffle arrangements, which is also equal to the external excitation frequency of the moving tank. The second peak frequency in Figure 9(a) is 1.0995 Hz, which is a little larger than the lowest theoretical natural frequency 1.0924 Hz. Similarly, the second peak frequencies 0.7664, 0.8329, and 0.8996 Hz in Figures 9(b)–9(d) would be also near each natural frequency of tank-liquid system with other three different combinatorial baffles. It is observed from the power spectrum that the natural frequency can be reduced by installing the baffles into the tank. Moreover, the natural frequency increases with increasing the perforated area for tank with orifice vertical baffle.

The total wave energy E_T can be obtained by the integration of flows properties under a linear wave, which is proportional to square of wave height H, namely, $E_T = \rho g H^2/8$ [24]. The maximum free surface elevation before the sloshing wave possibly breaks up at the wave gauge $G1$ $\eta_{\max}$ is taken as the maximum wave amplitude. Therefore, the maximum slosh-induced wave energy E_S is proportional to square of $\eta_{\max}$, namely, $E_S \propto \eta_{\max}^2$. The energy dissipation ratio ξ can be simply defined as follows: $\xi = (E_S - E_B)/E_S \times 100\% = (\eta_{\max S}^2 - \eta_{\max B}^2)/\eta_{\max S}^2 \times 100\%$, where E_B, $\eta_{\max B}$ is the maximum slosh-induced wave energy and free surface elevation when antisloshing baffle is installed into the tank, respectively. In fact, the energy dissipation ratio depends on the excitation amplitude, frequency, filling level, liquid viscosity, tank dimensions, and so forth. In the simulation of $\omega = 6.8636$ rad/s, which is equal to the lowest theoretical natural frequency, simulation results of the free surface elevation at three wave gauges for different baffle arrangements are shown in Figure 10. It is obviously observed from the plot that the maximum free surface elevation can be significantly reduced by using the nonconventional combinatorial baffles. The energy dissipation ratio is 99.73% for the case in Figure 10(b), 99.71% for the case in Figure 10(c) and 99.25% for the case in Figure 10(d), respectively. It is also seen that the size of the orifice has a slight influence on the sloshing magnitude when the free surface does not pass through the orifice. It should be valuable that the orifice allowed partial liquids to pass through freely, and the dynamic pressure loads acting on the baffles are hereby lessened.

In order to exhibit the liquid sloshing phenomena in cubic tank with multiple baffles, the snapshots of liquid sloshing in cubic tank without and with the perforated combinatorial baffles with $b = 80$ mm in orifice dimension at $t = 8.90$, 9.05, 9.15, 9.25, and 9.40 s are plotted in Figure 11, which also shows that the liquid sloshing amplitude is obviously reduced. In practice, the optimum design of baffle perforation should be more carefully checked by experiment and numerical simulation.

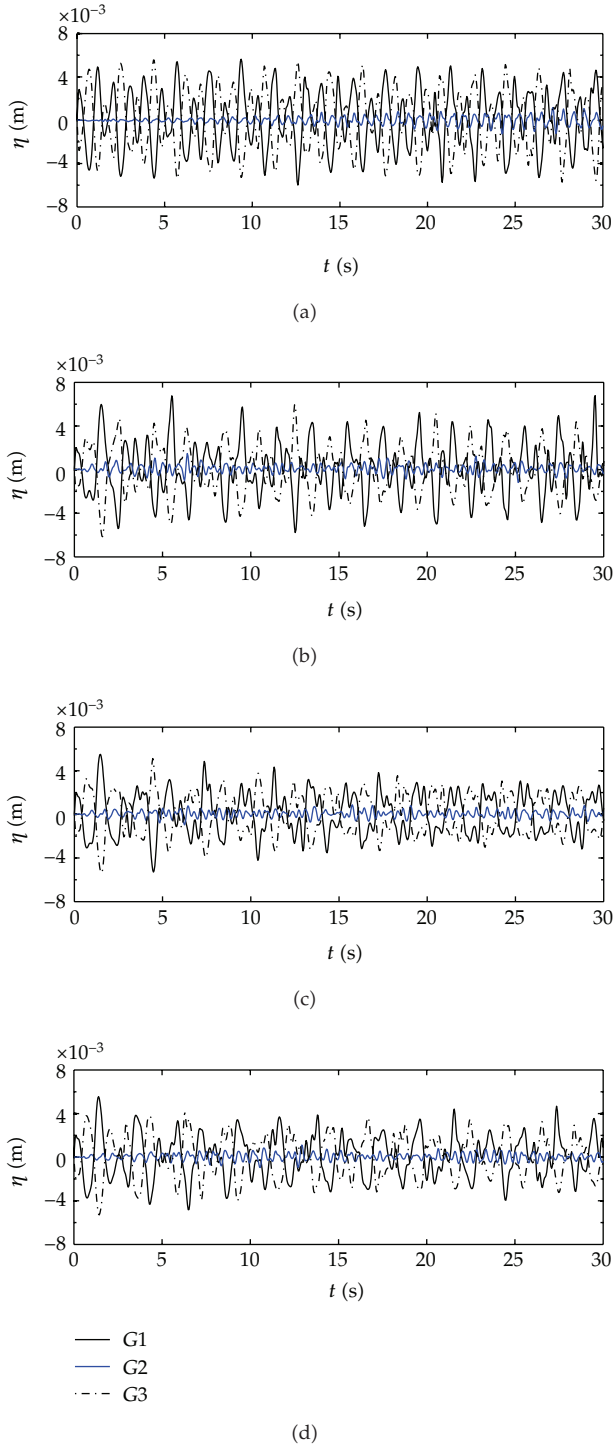

Figure 8: Comparisons of the free surface elevation at three wave gauges among the different baffle arrangements under the excitation of $\omega = \pi$ rad/s ((a) without baffle; (b) $b = 0$ mm; (c) $b = 40$ mm; (d) $b = 80$ mm).

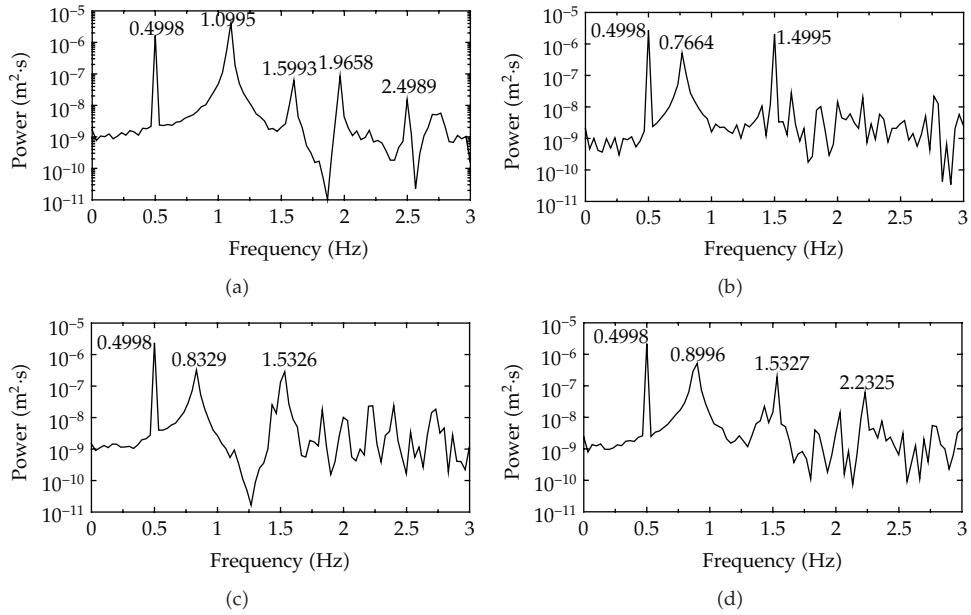

Figure 9: Power spectrum of the free surface elevation at wave gauge $G1$ when the excitation frequency is $\omega = \pi$ rad/s ((a) without baffle; (b) $b = 0$ mm; (c) $b = 40$ mm; (d) $b = 80$ mm).

Figure 12 shows the power spectrum of the time series of the free surface elevation at wave gauge $G1$ under the higher external excitation frequency for liquid sloshing in a tank with different baffle arrangements. It is observed from Figure 12 that the total energy is remarkably dissipated due to the presence of the combinatorial baffles in spite of the size of the orifice. For tank with the combinatorial baffles, the first peak frequency is equal to the external excitation frequency of the moving tank. However, the natural frequency does not appear in power spectrum when the external excitation frequency is larger than the natural frequency. In terms of engineering application and damping effectiveness of the baffles, the appropriate orifice baffles have particular advantages of being lightweight and enabling the large-scale tanker payload to be increased without compromising safety.

4.3. Dynamic Pressure Distribution under Resonant Frequency Excitation

4.3.1. Pressure Acting on the Sidewall Normal to the Motion of the Tank

The accurate prediction of dynamic pressure loads under the resonant frequency excitation is essential for the design of liquid storage containers. Figure 13 shows the dynamic pressure distribution acting on the sidewall normal to the motion of the tank. It is found that the dynamic pressure loads increase with the pressure measurement point being near the free surface, that is, $P1 < P2 < P3$ for liquid sloshing in a tank without baffle, whereas the dynamic pressure distribution is varying with installing the different combinatorial baffles inside the tank but tallies with the following rules, that is, $P2 < P1 < P3$.

As observed in the power spectrum of the time series of the free surface elevation, the lowest sloshing frequency has a remarkable change by using baffles in liquid tanks. The severe degree of sloshing motion and its accompanying dynamic pressure loads sensitively

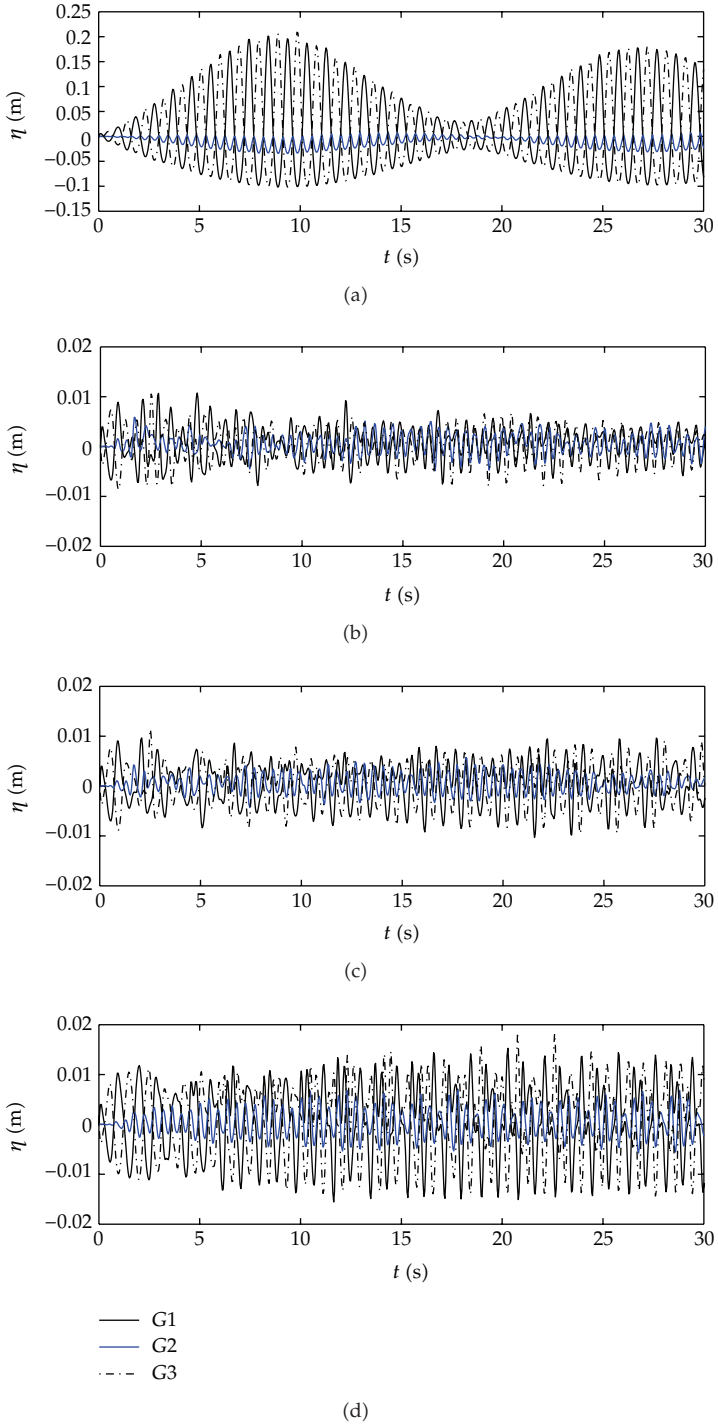

Figure 10: Comparisons of the free surface elevation at three wave gauges among the different baffle arrangements under the excitation of $\omega = 6.8636$ rad/s ((a) without baffle; (b) $b = 0$ mm; (c) $b = 40$ mm; (d) $b = 80$ mm).

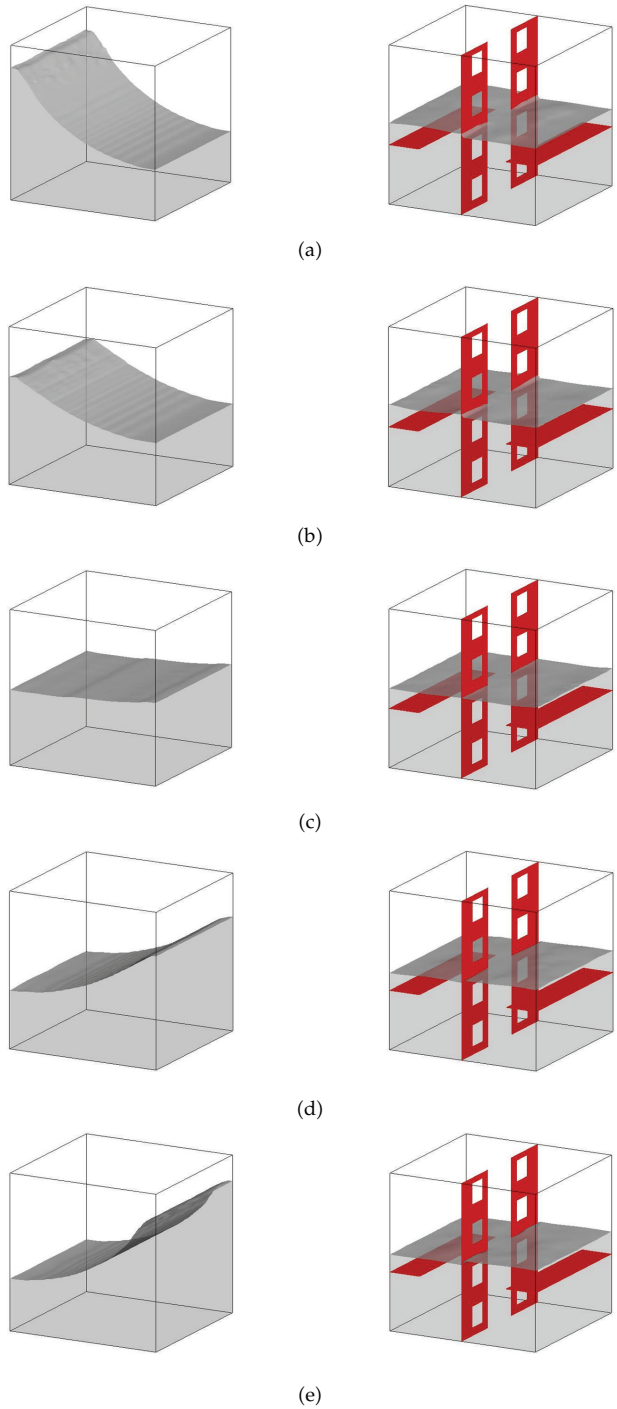

Figure 11: Snapshots of liquid sloshing in cubic tank without and with multiple baffles at t = 8.90, 9.05, 9.15, 9.25, and 9.40 s.

Table 1: The maximum dynamic pressure acting on the tank sidewalls for the different combinatorial baffles installed inside the tank.

Dynamic pressure $P_{\max}$(KPa)	Without baffle	$b = 0$ mm	$b = 40$ mm	$b = 80$ mm
$P1$	0.6262	0.0401	0.0355	0.0457
$P2$	0.6502	0.0377	0.0339	0.0445
$P3$	0.7169	0.0683	0.0684	0.0973
$P4$	0.4149	0.0592	0.0490	0.0347
$P5$	0.3522	0.0719	0.0604	0.0454
$P6$	0.1694	0.1041	0.0920	0.0706

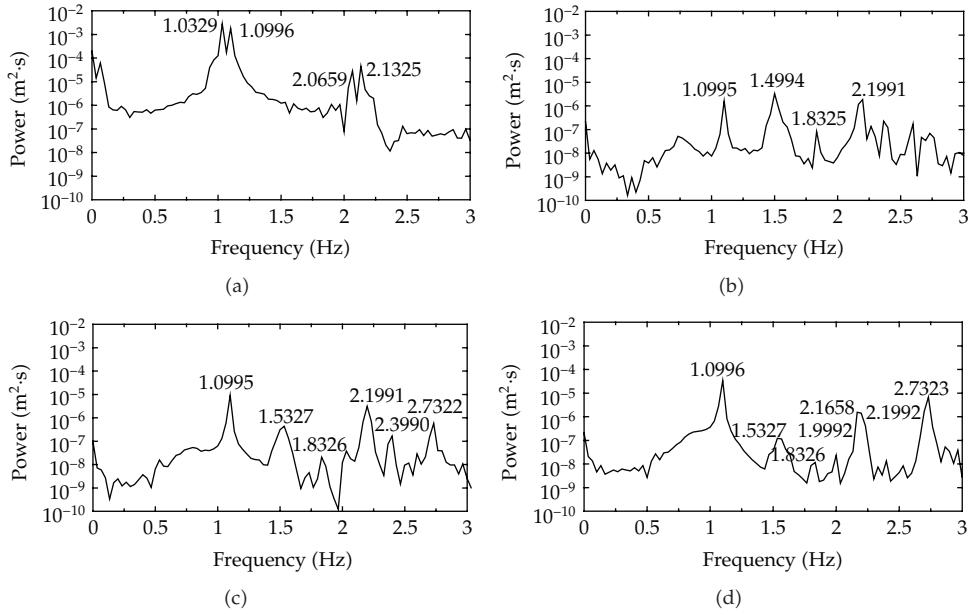

Figure 12: Power spectrum of the free surface elevation at wave gauge $G1$ when the excitation frequency is $\omega = 6.8636$ rad/s ((a) without baffle; (b) $b = 0$ mm; (c) $b = 40$ mm; (d) $b = 80$ mm).

depend on the relations between the natural frequency of tank-liquid system and external excitation frequency. Therefore, baffle damping mechanisms are relative to the variation of flow fields and natural frequency induced by the baffles. In this study, the magnitude of the dynamic pressure peaks at $P3$ is seen to decrease by 90.47% for $b = 0$ mm, 90.46% for $b = 40$ mm, and 86.43% for $b = 80$ mm compared with the without baffle case, indicating that the orifice baffle with $b = 40$ mm is not only lessening the baffles weight but also very effective in reducing the slosh-induced impact pressure. The maximum dynamic pressure at $P1$, $P2$, and $P3$ is summarized in Table 1.

4.3.2. Pressure Acting on the Sidewall Parallel to the Motion of the Tank

Figure 14 shows the dynamic pressure acting on the sidewall parallel to the motion of the tank. The positions of these pressure measurement points are shown in Figure 7. It is found that the dynamic pressure loads decrease with the pressure measurement point being near

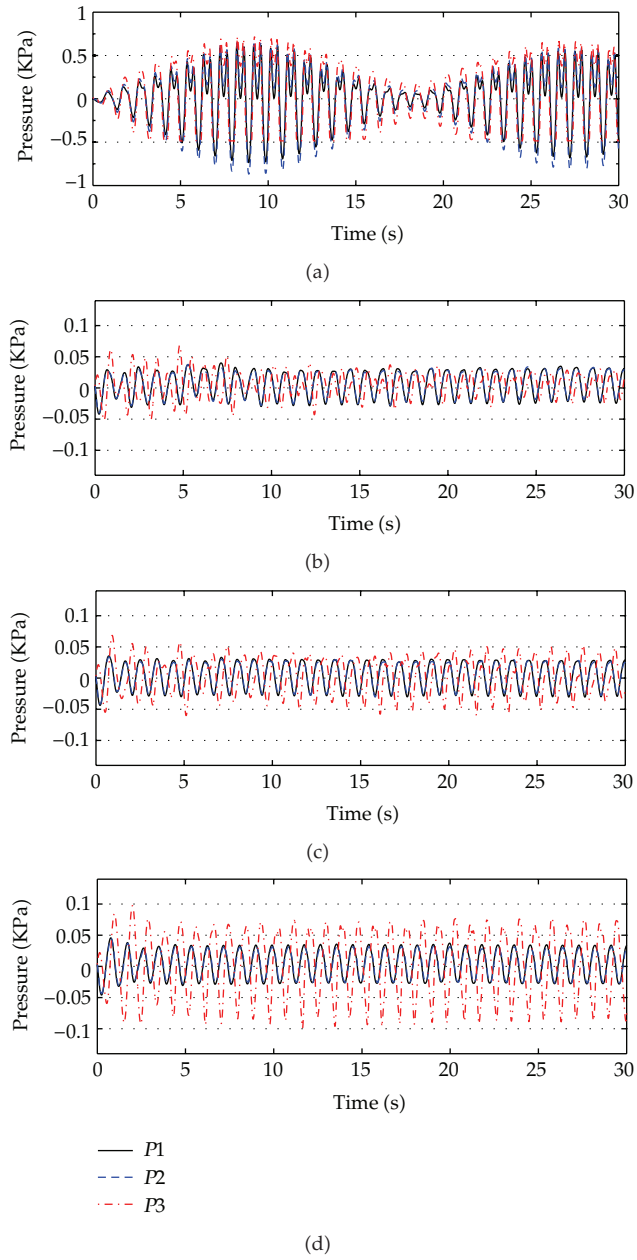

Figure 13: Dynamic pressure acting on the sidewall normal to the motion of the tank ((a) without baffle; (b) $b = 0$ mm; (c) $b = 40$ mm; (d) $b = 80$ mm).

the free surface, that is, $P4 > P5 > P6$ for liquid sloshing in a tank without baffle, whereas the dynamic pressure distribution is changed to be $P4 < P5 < P6$ when the different combinatorial baffles were installed into the tank. It can be also observed from Figure 14 that the dynamic impact pressure decreases with the increasing perforated area of the orifice baffle for all the pressure measurement points located on the sidewall parallel to the motion of the tank.

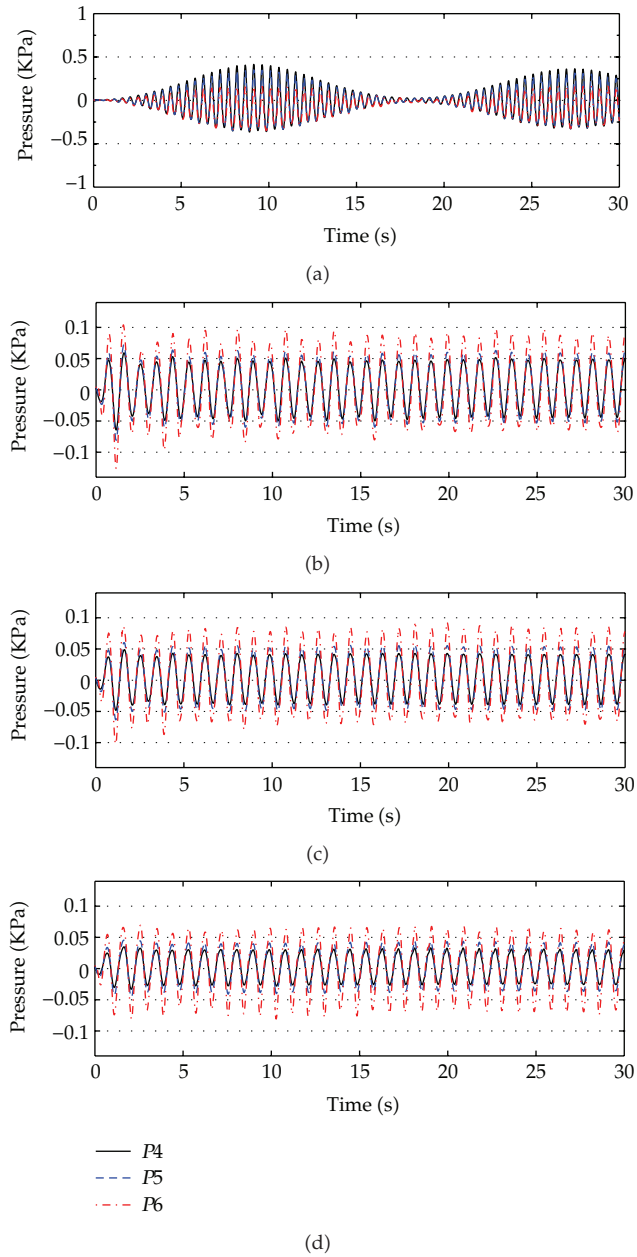

Figure 14: Dynamic pressure acting on the sidewall parallel to the motion of the tank ((a) without baffle; (b) $b = 0$ mm; (c) $b = 40$ mm; (d) $b = 80$ mm).

The maximum dynamic pressure acting on the tank wall can be also found in Table 1. For the case of $b = 80$ mm, the maximum dynamic impact pressure at $P4$, $P5$, and $P6$ is reduced by 91.64%, 87.11%, and 58.32% respectively, compared with the without baffle case. It is clearly observed from Table 1 that the maximum dynamic impact pressure acting on the parallel sidewall is far lower than that acting on the normal sidewall for the same position

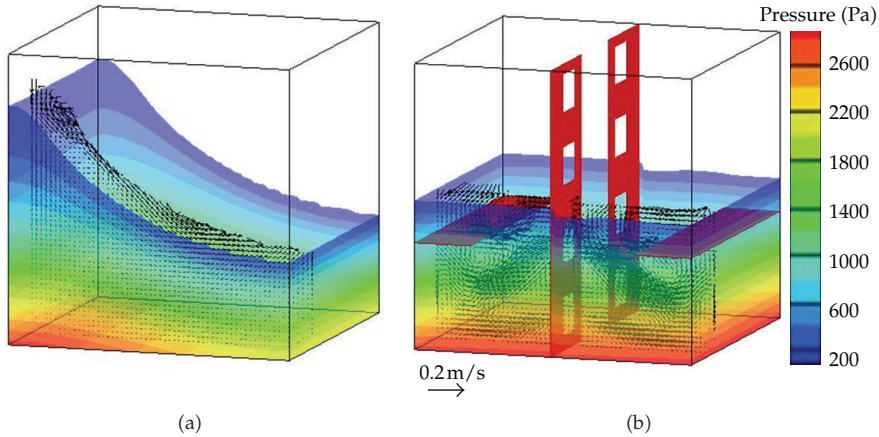

Figure 15: Velocity vectors through center line of one orifice vertical baffle and pressure distributions acting on the tank wall at $t = 8.90$ s.

above the base of tank for without baffle case, whereas a marked difference of pressure distribution on the tank walls is reduced by using the combinatorial baffles. Typical pressure distributions and velocity vectors can be found in Figure 15. The sloshing liquid can, in general, create two types of dynamic pressure, that is, impulsive and nonimpulsive pressures [14]. In this study, the dynamic pressures acing on the normal wall are similar to impulsive pressures, which are rapid pressure pulses due to the impact between the liquid and the tank wall. The dynamic pressures acing on the parallel wall are similar to nonimpulsive pressures, which are the ordinary dynamic pressures in an oscillating fluid. Based on the previous studies, it can be concluded that the most severe dynamic impact pressures occur near the free surface.

5. Conclusions

A two-phase fluid flow code is employed to simulate 3D liquid sloshing phenomena in cubic tank with complex baffles such as perforated vertical baffle. A new laboratory experiment of 3D liquid sloshing in cubic tank with perforated baffle is conducted under surge excitation to validate the present numerical model. The model is also validated against the available numerical data of sloshing in a rectangular tank with horizontal baffle. Fairly good agreements are obtained.

It is found from our investigations that the most severe dynamic impact pressures frequently occur near the free surface. Moreover, the maximum dynamic impact pressure acting on the parallel sidewall is lower than that acting on the normal sidewall for the same height pressure monitoring point on the tank wall for without baffle case. The use of the nonconventional combinatorial baffles not only remarkably reduces the sloshing amplitude and dynamic impact pressures acting on the tank wall but also shifts the natural frequency of liquid storage tank system, which can be observed from the power spectrum of the free surface elevation time series. Although the appropriate orifice baffle has the advantage of being lightweight and enabling the large-scale tanker payload to be increased without compromising safety, the optimum design of baffle perforation should be more carefully checked by experiment and/or numerical simulation in next reports.

Acknowledgments

The research was supported by research grants from China Postdoctoral Science Foundation funded project (2012M511192), National Nature Science Foundation of China (51061130547), the Special Fund of State Key Laboratory of Hydrology-Water Resources and Hydraulic Engineering of China (2009585812), the Fundamental Research Funds for the Central Universities (Hohai University 2012B06514), the Priority Academic Program Development of Jiangsu Higher Education Institutions (Coastal Development and Conservancy), Ministry of Education's Academic Youth Award for Doctoral Candidate, and the 111 project (B12032).

References

[1] R. Ibrahim, *A Liquid Sloshing Dynamics: Theory and Applications*, Cambridge University, New York, NY, USA, 2005.

[2] A. Cariou and G. Casella, "Liquid sloshing in ship tanks: a comparative study of numerical simulation," *Marine Structures*, vol. 12, no. 3, pp. 183–198, 1999.

[3] O. M. Faltinsen, "A numerical nonlinear method of sloshing in tanks with two-dimensional flow," *Journal of Ship Research*, vol. 22, no. 3, pp. 193–202, 1978.

[4] H. M. Koh, J. K. Kim, and J. H. Park, "Fluid-structure interaction analysis of 3-D rectangular tanks by a variationally coupled BEM-FEM and comparison with test results," *Earthquake Engineering and Structural Dynamics*, vol. 27, no. 2, pp. 109–124, 1998.

[5] B. F. Chen and H. W. Chiang, "Complete two-dimensional analysis of sea-wave-induced fully nonlinear sloshing fluid in a rigid floating tank," *Ocean Engineering*, vol. 27, no. 9, pp. 953–977, 2000.

[6] F. T. Dodge, *The Dynamic Behavior of Liquids in Moving Containers*, Southwest Research Institute, San Antonio, Tex, USA, 2000.

[7] L. K. Forbes, "Sloshing of an ideal fluid in a horizontally forced rectangular tank," *Journal of Engineering Mathematics*, vol. 66, no. 4, pp. 395–412, 2010.

[8] G. H. Keulegan and L. H. Parkinson, "Forces on cylinders and plates in an oscillating fluid," National Bureau of Standards Report 4821, 1956.

[9] J. W. Miles, "Ring damping of free surface oscillations in a circular tank," *Journal of Applied Mechanics*, vol. 25, no. 2, pp. 274–276, 1958.

[10] V. Armenio and M. La Rocca, "On the analysis of sloshing of water in rectangular containers: numerical study and experimental validation," *Ocean Engineering*, vol. 23, no. 8, pp. 705–739, 1996.

[11] Y. Kim, "Numerical simulation of sloshing flows with impact load," *Applied Ocean Research*, vol. 23, no. 1, pp. 53–62, 2001.

[12] H. Akyildiz and M. S. Çelebi, "Numerical computation of pressure in a rigid rectangular tank due to large amplitude liquid sloshing," *Turkish Journal of Engineering and Environmental Sciences*, vol. 25, no. 6, pp. 659–674, 2001.

[13] M. S. Celebi and H. Akyildiz, "Nonlinear modeling of liquid sloshing in a moving rectangular tank," *Ocean Engineering*, vol. 29, no. 12, pp. 1527–1553, 2002.

[14] H. Akyildiz and E. Ünal, "Experimental investigation of pressure distribution on a rectangular tank due to the liquid sloshing," *Ocean Engineering*, vol. 32, no. 11-12, pp. 1503–1516, 2005.

[15] J. R. Cho, H. W. Lee, and S. Y. Ha, "Finite element analysis of resonant sloshing response in 2-D baffled tank," *Journal of Sound and Vibration*, vol. 288, no. 4-5, pp. 829–845, 2005.

[16] K. C. Biswal, S. K. Bhattacharyya, and P. K. Sinha, "Non-linear sloshing in partially liquid filled containers with baffles," *International Journal for Numerical Methods in Engineering*, vol. 68, no. 3, pp. 317–337, 2006.

[17] M. F. Younes, Y. K. Younes, M. El-Madah, I. M. Ibrahim, and E. H. El-Dannanh, "An experimental investigation of hydrodynamic damping due to vertical baffle arrangements in a rectangular tank," *Proceedings of the Institution of Mechanical Engineers Part M: Journal of Engineering for the Maritime Environment*, vol. 221, no. 3, pp. 115–123, 2007.

[18] P. K. Panigrahy, U. K. Saha, and D. Maity, "Experimental studies on sloshing behavior due to horizontal movement of liquids in baffled tanks," *Ocean Engineering*, vol. 36, no. 3-4, pp. 213–222, 2009.

[19] M. Eswaran, U. K. Saha, and D. Maity, "Effect of baffles on a partially filled cubic tank: numerical simulation and experimental validation," *Computers and Structures*, vol. 87, no. 3-4, pp. 198–205, 2009.

[20] D. Liu and P. Lin, "Three-dimensional liquid sloshing in a tank with baffles," *Ocean Engineering*, vol. 36, no. 2, pp. 202–212, 2009.
[21] R. Mittal and G. Iaccarino, "Immersed boundary methods," *Annual Review of Fluid Mechanics*, vol. 37, pp. 239–261, 2005.
[22] D. Liu and P. Lin, "A numerical study of three-dimensional liquid sloshing in tanks," *Journal of Computational Physics*, vol. 227, no. 8, pp. 3921–3939, 2008.
[23] P. Lin and C. W. Li, "Wave-current interaction with a vertical square cylinder," *Ocean Engineering*, vol. 30, no. 7, pp. 855–876, 2003.
[24] P. Lin, *Numerical Modeling of Water Waves*, Taylor & Francis, London, UK, 2008.
[25] M.-A. Xue and P. Lin, "Numerical study of ring baffle effects on reducing violent liquid sloshing," *Computers and Fluids*, vol. 52, no. 1, pp. 116–129, 2011.
[26] W. J. Rider and D. B. Kothe, "Reconstructing volume tracking," *Journal of Computational Physics*, vol. 141, no. 2, pp. 112–152, 1998.
[27] D. Liu, *Numerical modeling of three-dimensional water waves and their interaction with structures [Ph.D. thesis]*, National University of Singapore, 2007.